

Article

Improvement of PMSG-Based Wind Energy Conversion System Using Developed Sliding Mode Control

Btissam Majout¹, Badre Bossoufi^{1,*}, Manale Bouderbala¹, Mehedi Masud², Jihad F. Al-Amri³, Mohammed Taoussi¹, Mohammed El Mahfoud¹, Saad Motahhir⁴ and Mohammed Karim¹

¹ LIMAS Laboratory, Faculty of Sciences Dhar El Mahraz, Sidi Mohammed Ben Abdellah University, Fez 30000, Morocco; btissam.majour@usmba.ac.ma (B.M.); Manale.bouderbala@usmba.ac.ma (M.B.); medtaoussi@usmba.ac.ma (M.T.); medmahfoud@usmba.ac.ma (M.E.M.); mohammed.karim@usmba.ac.ma (M.K.)

² Department of Computer Science, College of Computers and Information Technology, Taif University, P.O. Box 11099, Taif 21944, Saudi Arabia; mmasud@tu.edu.sa

³ Department of Information Technology, College of Computers and Information Technology, Taif University, P.O. Box 11099, Taif 21944, Saudi Arabia; j.alamri@tu.edu.sa

⁴ Engineering, Systems and Applications Laboratory, ENSA, Sidi Mohammed Ben Abdellah University, Fez 30000, Morocco; saad.motahhir@usmba.ac.ma

* Correspondence: Badre.bossoufi@usmba.ac.ma

Abstract: In recent years, regulating a wind energy conversion system (WECS) under fluctuating wind speed and enhancing the quality of the electricity provided to the grid has become a hard challenge for many academics. The current research provides a better control strategy to decrease the occurrence of chattering phenomena. Combined with the Maximum Power Point Tracking (MPPT) strategy and a pitch angle control, the control is possible to increase the performance and the efficiency of the Permanent Magnet Synchronous Generator (PMSG) based Wind Energy Conversion System. This study attempts initially to regulate the generator and the grid side converter to track the wind speed reference established by the MPPT algorithm. And secondly, to relieve the chattering problem associated with the conventional sliding mode control (CSMC), the proposed sliding mode control (PSMC) is based on a novel smooth continuous switching control. Besides, the suggested sliding mode control stability is confirmed using Lyapunov's stability function. The complete system was evaluated in the MATLAB/Simulink (MathWorks, Natick, MA, USA) environment using a 2 MW PMSG's power, under random fluctuations in the wind speed to show the suggested approach's efficiency and robustness, which was then compared to the CSMC and other common approaches available in the literature. The simulation results reveal that the recommended sliding mode control approach delivers good speed, accuracy, stability, and output current's ripple.

Keywords: wind turbine; sliding mode control; electrical machine; power electronics; PMSG



Citation: Majout, B.; Bossoufi, B.; Bouderbala, M.; Masud, M.; Al-Amri, J.F.; Taoussi, M.; El Mahfoud, M.; Motahhir, S.; Karim, M. Improvement of PMSG-Based Wind Energy Conversion System Using Developed Sliding Mode Control. *Energies* **2022**, *15*, 1625. <https://doi.org/10.3390/en15051625>

Academic Editors: Hasmat Malik and Flavio Caresana

Received: 16 December 2021

Accepted: 14 February 2022

Published: 22 February 2022

Publisher's Note: MDPI stays neutral with regard to jurisdictional claims in published maps and institutional affiliations.



Copyright: © 2022 by the authors. Licensee MDPI, Basel, Switzerland. This article is an open access article distributed under the terms and conditions of the Creative Commons Attribution (CC BY) license (<https://creativecommons.org/licenses/by/4.0/>).

1. Introduction

Nowadays, substantial effort is being made to develop a source of renewable energy as a substitute for fossil fuels and to protect the environment [1]. As a result, wind energy technology has garnered significant attention in recent years due to various advantages, including low cost, ease of deployment, and low maintenance [2,3].

PMSG-based WECS are widely utilized in wind energy generation due to their small structure, high power density, and high torque-inertia ratio. Additionally, the PMSG's internal structure, which incorporates precision gears and brushes, is simplified compared to the doubly-fed induction generator (DFIG). As a result of this development, WECS based on PMSG has become a research hotspot in wind energy generating [4].

However, due to the randomness and unpredictability of wind energy's wind speed, current research on high-power wind generators frequently fails to attain their full output.

As a result, they decreased the efficiency of wind energy usage and nullified the benefits of high-power wind generators. On the other hand, because wind speeds fluctuate often and wind energy is inherently unstable, the grid connection of large-capacity wind farms may introduce specific shocks into the large-power system, rendering it unstable.

To minimize the cost of wind energy generation, the wind farm's wind energy conversion efficiency must be increased. As a result, it becomes more critical to improving the wind energy system's control mechanism. At rated wind speeds, modern WECS frequently use the best characteristic curve as the control mechanism for MPPT. It is capable of varying the mechanical output of the generator in response to the wind turbine's input under varying weather conditions. As a result, the WECS maintains an optimal blade Tip Speed Ratio (TSR) to maximize wind energy capture.

Wind turbines, on the other hand, capture wind energy based on a variety of parameters. Wind speed, blade pitch angle, and wind wheel rotation speed all affect the amount of wind energy captured. In addition, the randomness of wind variations and energy loss in WECS will affect the WECS's stability [5]. As a result, converting wind energy to electrical energy is not a linear process that often involves significant disturbance and uncertainty. Over the last few decades, numerous control theories and strategies have been proposed in the literature to address the aforementioned PMSG issues [6]. The primary control objectives are to maximize power extraction and regulate reactive power to the desired power factor according to grid needs. These tasks must be accomplished concurrently using an appropriate voltage vector. The global model of the WECS based PMSG is presented in Figure 1.

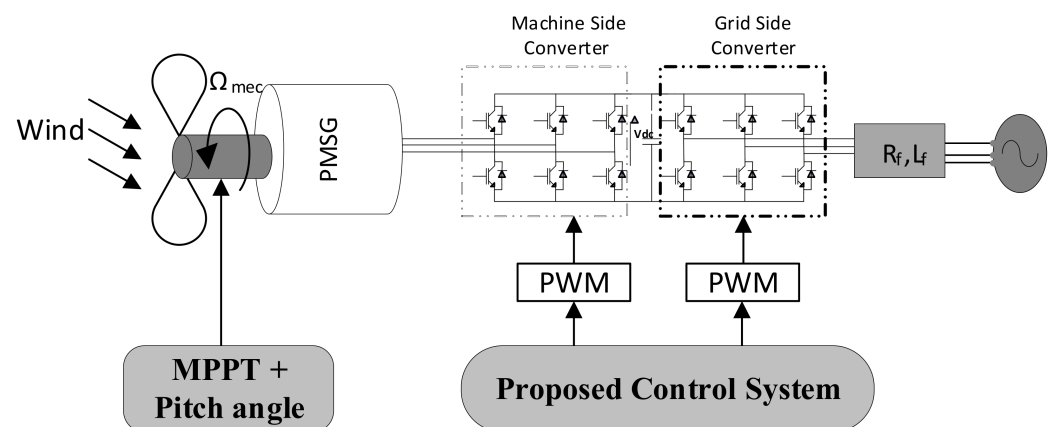


Figure 1. WECS global model.

Due to the benefits of a simple control algorithm, high reliability, and simplicity of implementation, in reality, the Proportional Integral (PI) control technique is often used to enhance the system reliability of the rotor side converter (RSC) and grid side converter (GSC) of the PMSG wind turbine. The PI controller is used in [7] to optimize the PMSG wind turbine's performance in both windy and steady-state circumstances. However, the PI control scheme, which is a linear control approach, is not robust enough to react to the nonlinearity of the PMSG wind turbine system and variations in wind speed and wind turbine parameters. Consequently, several nonlinear control schemes have been developed and applied in wind turbine systems to enhance power quality, including fuzzy control [8,9], backstepping control [10–12], and direct power control (DPC). However, fuzzy control is tough to execute in reality as it demands extensive expert knowledge and human cognition, resulting in a delayed response in exchange for high accuracy. While the DPC gives great transient responsiveness, it needs a high switching frequency to reduce torque/current ripples [13]. Backstepping control has the inherent issue of generating an “explosion of complexity”, lowering the controller's performance.

Apart from the nonlinear control systems previously treated, sliding mode control (SMC) has gained substantial interest because of its organisation's effectiveness, quick reaction, simplicity of implementation, and low susceptibility to parameter changes [14,15]. SMC is a sort of nonlinear resilient control that is immune to parameter changes. In recent years, it has garnered considerable interest for WECS control due to its ease of implementation, order reduction, and tolerance for external disturbances and parametric perturbations, including suitable wind energy extraction, Direct Current (DC) link wattage maintenance, and direct wind energy power management.

The first order Sliding mode control (SMC) is applied to manage both the speed and power of the PMSG-based WECS in [16–18]. Typically, the current control generates a voltage reference in real-time using the pulse-width modulation (PWM) technique. As a result, the voltage reference cannot be followed precisely using the PWM technique when the sign function is employed due to the chattering phenomena. In [19,20], continuous approximation and a saturation function were used to construct SMC with reduced chattering for PMSG-based WECS. Regrettably, when a saturation function is used, a finite steady-state error is produced. The authors of [11,21] describe a way for improving the output power quality of a permanent magnet synchronous generator (PMSG) using fractional-order sliding mode control (FOSMC); nevertheless, this method requires precise adjustment of the fractional operator. The authors of [19] investigated an approach for adaptive second-order SMC (SOSMC). This strategy can effectively deal with model uncertainty, WECS's inherent nonlinear behavior, and random wind. However, the usage of differentiators, whose actual behavior needs further caution when implemented due to measurement noise. Meanwhile, [22,23] discussed the I-SMC (integral sliding-model control) technique for high-precision steady-state control. Nevertheless, the controller's gain must be carefully adjusted to strike a balance between strength and chattering. SOSMC is used in conjunction with the Super Twisting (ST) algorithm in [21]. While ST can produce a quick transient response with zero steady-state error, it typically results in excessive controller gains, resulting in chattering.

The fundamental disadvantage of SMC approaches is chattering, produced by the discontinuous control law utilized in the construction of the SMC and parasitic dynamics interactions. Chattering can damage the system because it reduces control accuracy, resulting in more significant heat loss in electrical power circuits and higher wear on mechanical components that move.

This article discusses the control design of PMSG. The peculiarity of this study is that it presents a novel controller structure that is distinct from the majority of sliding mode control-based PMSG wind turbine systems. PMSG incorporates a novel sliding mode controller that is based on a new approach rate. The controller can sustain steady transient performance in the presence of external disturbances, reduce the load associated with electrical energy generation, and enhance the quality of electrical energy delivered. Additionally, a new smooth continuous switching control has been presented to smooth the signal to solve the previously noted chattering and discontinuous function. This technique works by replacing the typical discontinuous function in the switching control with a smooth continuous function.

The remaining of this paper is prepared as follows: Section 2 is devoted to the dynamic model of the wind energy conversion system (WECS), as well as the MPPT strategy and the pitch control while Section 3 discusses the proposed sliding mode control. In Section 4, the performances results of the SMC control are presented and analyzed, and then compared with other controls' results.

2. Wind Power System Model

2.1. Wind Turbine Model

The model of wind power is [24,25]:

$$P_{wind} = \frac{1}{2} \times \rho \times S \times v_w^3 \quad (1)$$

$$P_{turb} = C_p(A, \beta) \times P_{wind} = \frac{1}{2} \times \rho \times S \times C_p(A, \beta) \times v_w^3 \tag{2}$$

$$T_{turb} = \frac{P_{turb}}{\Omega_t} = \frac{1}{2} \times \varphi \times S \times C_p(A, \beta) \times v_w^3 \times \frac{1}{\Omega_t} \tag{3}$$

where C_p is a power coefficient adopted to the wind turbine [2–24]:

$$\left\{ \begin{array}{l} C_p(A, \beta) = 0.5176 \left(\frac{116}{A} - 0.4\beta - 4 \right) \times e^{-\frac{21}{A}} + 0.0068 \times \lambda \\ \frac{1}{A} = \frac{1}{\lambda + 0.08\beta} - \frac{0.035}{1 + \beta^3} \\ \lambda = \frac{\Omega_t \times R}{V_w} \\ C_p^{max}(\lambda, \beta) = \frac{16}{27} = 0.5930 \end{array} \right. \tag{4}$$

2.2. Maximum Power Extraction

The MPPT control strategy generally aims to extract the maximum available power in the wind and run the generator at its optimum speed by adjusting the rotational speed of the wind turbine for any wind speed below the rate value. This optimum is obtained when $\lambda_{opt} = 8$ and $\beta = 0^\circ$ [3–22]. To achieve this, the electromagnetic torque must be regulated and estimated through the MPPT technique and then applied to the PMSG to ensure that the wind turbine rotates at its specific speed. Its expression becomes as follows [25,26]:

$$T_{em_ref} = \frac{P_{turb-ref}}{\Omega_t} = \frac{\rho \times \pi \times R^5 \times C_{p_max}(\lambda_{opt}) \times \Omega_{mec}^2}{2 \times \lambda_{opt}^3} \tag{5}$$

Figure 2 explains the principle of operation of the MPPT command.

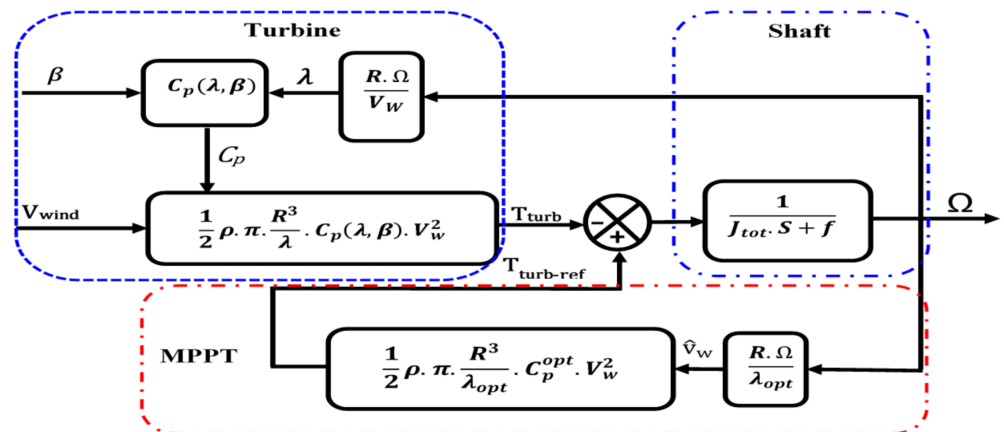


Figure 2. Turbine and MPPT model.

In addition, to guarantee wind turbine system protection and safety, and maintain the power at its rated value, a mechanical technique called the pitch angle control is usually used to adjust the pitch angle of the blades according to the wind speed. This technique limits the output power and the speed once the generator speed exceeds 30% of its rated speed [5,27,28]. Figure 3 shows the pitch angle control structure.

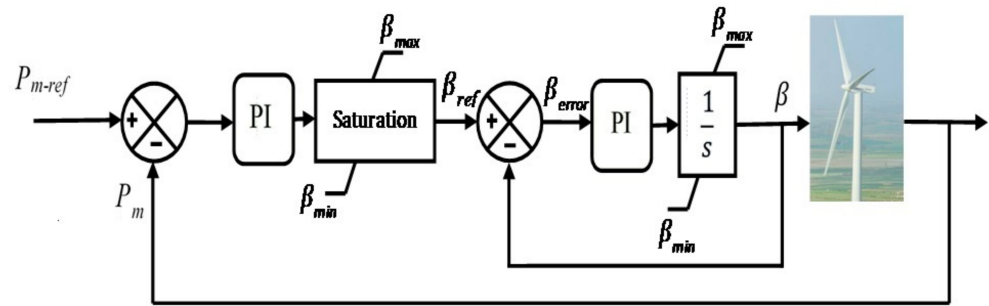


Figure 3. Block diagram of the pitch angle control.

2.3. Permanent Magnet Synchronous Generator Model

The model of the PMSG is defined in the d - q synchronous reference, as follows [1,29,30]:

$$\frac{dI_{sd}}{dt} = - \left[\frac{R_s}{L_d} \times I_{sd} - \omega_e \times \frac{L_q}{L_d} \times I_{sq} - \frac{V_{sd}}{L_d} \right] \quad (6)$$

$$\frac{dI_{sq}}{dt} = - \left[\frac{R_s}{L_q} \times I_{sq} + \omega_e \times \frac{L_d}{L_q} \times I_{sd} - \omega_e \times \frac{\varnothing_f}{L_q} + \frac{V_{sq}}{L_q} \right] \quad (7)$$

$$\omega_e = p \times \Omega_{mec} \quad (8)$$

$$\begin{cases} \Psi_{sd} = L_d \times i_{sd} + \varnothing_f \\ \Psi_{sq} = L_q \times i_{sq} \end{cases} \quad (9)$$

$$T_{em} = \frac{3}{2} \times p \left[(L_d - L_q) I_{sd} \times I_{sq} + I_{sq} \times \varnothing_f \right] \quad (10)$$

$$\frac{d\Omega_{mec}}{dt} = \frac{1}{J_{tot}} \times T_{turb} - \frac{3}{2} \times \frac{p}{J_{tot}} \times I_{sq} \times \varnothing_f - \frac{f}{J_{tot}} \times \Omega_{mec} \quad (11)$$

$$P_{gen} = \frac{3}{2} [V_{sd} \times I_{sd} + V_{sq} \times I_{sq}] \quad (12)$$

$$Q_{gen} = \frac{3}{2} [V_{sq} \times I_{sd} - V_{sd} \times I_{sq}] \quad (13)$$

2.4. Filter (R, L) and Grid Model

The dynamic model of the grid side converter in the d - q reference frame can be presented as follows [2,31]:

$$\begin{cases} \frac{dI_{gd}}{dt} = \left[\frac{v_{fd}}{L_f} - \frac{R_f}{L_f} \times I_{gd} + \omega_g \times I_{gq} - \frac{v_{gd}}{L_f} \right] \\ \frac{dI_{gq}}{dt} = \left[\frac{v_{fq}}{L_f} - \frac{R_f}{L_f} \times I_{gq} - \omega_g \times I_{gd} - \frac{v_{gq}}{L_f} \right] \end{cases} \quad (14)$$

where V_{fd} and V_{fq} are the inverter d - q axis voltage components, and L_f and R_f are the inductance and the resistance of the grid side filter, respectively, connected in series.

The active and reactive powers of the grid can be expressed as follows:

$$P_g = \frac{3}{2} [V_{gd} \times I_{gd} + V_{gq} \times I_{gq}] \quad (15)$$

$$Q_g = \frac{3}{2} [V_{gq} \times I_{gd} - V_{gd} \times I_{gq}] \quad (16)$$

A DC-link links the generator side converter with the grid side converter. Using the power balancing concept and omitting the converter losses, the dynamic behavior of the DC-link voltage can be stated as follows [23,32]:

$$P_{gen} - P_g = \frac{1}{2} \times C \times \frac{dv_{DC}^2}{dt} \quad (17)$$

3. Synthesis of Control

3.1. Description Model

When the wind speed changes, the active and reactive power, voltage, and frequency injected into the grid must be adjusted by controlling the frequency converters, which consist of a pulse width modulation (PWM) rectifier and a PWM inverter [33–35], in order to achieve the desired control objectives. As a result, the state vector and control vector are selected in the following manner:

$$[X] = [I_{sd}, I_{sq}, \Omega_{mec}, I_{gd}, I_{gq}]^T \text{ is the state vector.}$$

$$[U] = [V_{sd}, V_{sq}, V_{fd}, V_{fq}]^T \text{ is the control variable.}$$

3.2. Sliding Mode Controller Design

Generally, the sliding mode control aims to force the system to slide along the pre-designed sliding mode surface in finite time and then stay there despite uncertainties, e.g., wind speed uncertainties or parameter uncertainties of the system, where the system is dynamic. The latter allows the system to switch between differentiators, and is altered by using a discontinuous control signal structure at any time. In this case, the system dynamic combines the beneficial properties of each of these structures to achieve the desired system behavior [24,36]. However, the ordinary SMC suffers from chattering and reaching the phase instability problem [29,37]. Therefore, an SMC control strategy has been proposed to solve the common SMC problems and improve the system's performance [33,34]. This technique is characterized by its simplicity and efficiency.

In the proposed SMC control scheme, the chosen sliding surface is as follows [38]:

$$S(X) = \left(\frac{d}{dt} + \delta \right)^{n-1} \times e(x) \quad (18)$$

where n denotes the order of the system, δ is a positive constant, and $e(x)$ is the error between the desired signal x_{ref} and the state variable x .

By choosing $n = 1$, the tracking error dynamics of the proposed sliding surface becomes the following:

$$S(X) = e(x) = x_{ref} - x \quad (19)$$

Furthermore, the first order SMC includes two terms (U_{eq} and U_n), where U_{eq} is an equivalent control that characterizes the system's behavior on the sliding surface, whereas U_n is a switching control based on a discontinuous function (sign). It is employed to satisfy the condition of attractiveness and stabilization [28–32]. Therefore, to attain commutation around the surface of PSMC, each component of the control approach is calculated as the addition of two terms [24–39], as follows:

$$U_c = U_{eq} + U_n \quad (20)$$

where the expression of the switching signal U_n is determined as follows:

$$U_n = K_n \operatorname{sgn}(S_n) \quad (21)$$

K_n is a positive switching gain that is selected to attain the optimum performance and minimize the dynamic system disturbance. $\operatorname{sgn}(S_n)$ is a discontinuous mathematical

function characterized by an imperfect switching that causes the control signal to chatter [31]. To reduce this phenomenon, a new smooth continuous switching control has been proposed to smooth the signal. The principle of this technique is based on replacing the ordinary discontinuous function (Sign) in the switching control with a smooth continuous function as follows [31,40]:

$$U_n = K_n \times \text{Smooth}(S_n) \quad (22)$$

where $\text{Smooth}(S(X))$ is a smooth continuous function defined by the following:

$$\text{Smooth}(\lambda', S) = \frac{\lambda' S}{|\lambda' S| + \varepsilon} \quad (23)$$

ε is a small positive of the boundary layer width and λ' is a positive constant used to adjust the tuning rate of the function. These two parameters (ε, λ') determine the steepness of the continuous function. Moreover, the state-dependent boundary layer ε is designed as follows:

$$\varepsilon = (1 - |\text{Smooth}(\lambda', S)|) + \delta_1 \quad (24)$$

where δ_1 is a small positive constant.

3.2.1. Machine Side Converter Control MSC

On this side, three controllers, using the sliding mode, are designed to control the direct and quadrature current components of the stator (I_{sd}, I_{sq}) and the speed (Ω_{mec}).

The sliding surfaces have been fixed as follows [41]:

$$S(I_{sd}) = e(I_{sd}) = I_{sd}^* - I_{sd} \quad (25)$$

$$S(I_{sq}) = e(I_{sq}) = I_{sq}^* - I_{sq} \quad (26)$$

$$S(\Omega_{mec}) = e(\Omega_{mec}) = \Omega_{mec}^* - \Omega_{mec} \quad (27)$$

where I_{sd}^* and I_{sq}^* are the references of the direct and the quadrature stator current, respectively, and Ω_{mec}^* is the mechanical speed reference.

Applying the time derivative to $S(I_{sd})$, $S(I_{sq})$ and $S(\Omega_{mec})$, the resulting equations are as follows:

$$\dot{S}(I_{sd}) = \dot{I}_{sd}^* + \frac{R_s}{L_d} \times I_{sd} - \omega_e \times \frac{L_q}{L_d} \times I_{sq} - \frac{V_{sd}}{L_d} \quad (28)$$

$$\dot{S}(I_{sq}) = \dot{I}_{sq}^* + \frac{R_s}{L_q} \times I_{sq} + \omega_e \times \frac{L_d}{L_q} \times I_{sd} + \omega_e \times \frac{\varnothing_f}{L_q} - \frac{V_{sq}}{L_q} \quad (29)$$

$$\dot{S}(\Omega_{mec}) = \dot{\Omega}_{mec}^* + \frac{f}{J_{tot}} \times \Omega_{mec} + \frac{\mu}{J_{tot}} \times I_{sq} - \frac{1}{J_{tot}} \times T_{turb} \quad (30)$$

With $\mu = \frac{3}{2} \times p \times \varnothing_f$. The sliding mode occurs on the sliding surface when the invariance conditions of the sliding surface are ensured, ($\dot{S}(X) = 0$) and ($V_{sd,qN} = 0$) [42]. Hence, the equivalent control expression $V_{sd,q_{eq}}$ for each axis is deduced from Equations (28) and (29). Thus,

$$V_{sd_{eq}} = L_d \left[\dot{I}_{sd}^* + \frac{R_s}{L_d} \times I_{sd} - \omega_e \times \frac{L_q}{L_d} \times I_{sq} \right] \quad (31)$$

$$V_{sq_{eq}} = L_q \left[\dot{I}_{sq}^* + \frac{R_s}{L_q} \times I_{sq} + \omega_e \times \frac{L_d}{L_q} \times I_{sd} + \omega_e \times \frac{\varnothing_f}{L_q} \right] \quad (32)$$

Whereas the switching control expressions V_{sd_N}, V_{sq_N} are defined as follows:

$$V_{sd_N} = K_d \times \text{Smooth}(S(I_{sd})) \text{ with } K_d > 0 \quad (33)$$

$$V_{sq_N} = K_q \times \text{Smooth}(S(I_{sq})) \text{ with } K_q > 0 \quad (34)$$

The overall control of each axis is as follows:

$$V_{sd_ref} = V_{sd_eq} + V_{sd_N} \tag{35}$$

$$V_{sq_ref} = V_{sq_eq} + V_{sq_N} \tag{36}$$

By using the above equations, the controller design of the generator side converter can be formed as follows:

$$V_{sd_ref} = L_d \left[\dot{I}_{sd}^* + \frac{R_s}{L_d} \times I_{sd} - \omega_e \times \frac{L_q}{L_d} \times I_{sq} \right] + K_d \times Smooth(S(I_{sd})) \tag{37}$$

$$V_{sq_eq} = L_q \left[\dot{I}_{sq}^* + \frac{R_s}{L_q} \times I_{sq} + \omega_e \times \frac{L_d}{L_q} \times I_{sd} + \omega_e \times \frac{\phi_f}{L_q} \right] + K_q \times Smooth(S(I_{sq})) \tag{38}$$

$$I_{sq}^* = I_{sq_eq} + I_{sq_N} \tag{39}$$

With,

$$\begin{cases} I_{sq_eq} = -\frac{I_{tot}}{\mu} \left[\dot{\Omega}_{mec}^* + \frac{f}{f_{tot}} \times \Omega_{mec} - \frac{1}{f_{tot}} \times T_{turb} \right] \\ I_{sq_N} = K_{\Omega_{mec}} \times Smooth(S(\Omega_{mec})) \text{ with } K_{\Omega_{mec}} > 0 \end{cases} \tag{40}$$

3.2.2. Grid Side Converter Control

To keep the DC-link voltage at a constant value, a PI controller was applied to regulate the voltage measured V_{DC} to track its reference V_{DC-ref} . Furthermore, to adjust the grid current frequencies and reach a unit power factor [43], two controllers using the sliding mode are designed to control the direct and quadrature current components (I_{gd}, I_{gq}) of the GSC, as shown in Figure 4.

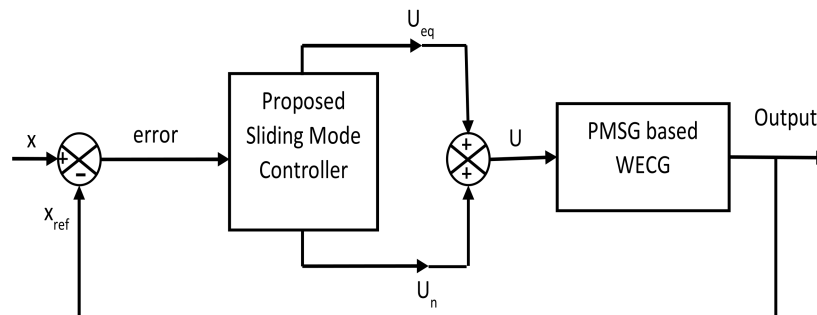


Figure 4. The general structure of the SMC.

On this side, the sliding surfaces have been fixed as follows:

$$S(I_{gd}) = e(I_{gd}) = I_{gd}^* - I_{gd} \tag{41}$$

$$S(I_{gq}) = e(I_{gq}) = I_{gq}^* - I_{gq} \tag{42}$$

I_{gd}^* and I_{gq}^* are the direct and the quadrature grid currents references.

Again, making use of the similar method used for the MSC control, the controller design of the grid side converter will be as follows:

$$V_{fd_ref} = V_{fd_eq} + V_{fd_N} \tag{43}$$

$$V_{fq_ref} = V_{fq_eq} + V_{fq_N} \tag{44}$$

$$\begin{cases} V_{fd_eq} = L_f \left[\dot{I}_{gd}^* + \frac{R_f}{L_f} \times I_{gd} - \omega_g \times I_{gq} + \frac{V_{gd}}{L_f} \right] \\ V_{fd_N} = K_{fd} \times Smooth(S(I_{rd})) \text{ with } K_{fd} > 0 \end{cases} \tag{45}$$

$$\begin{cases} V_{fq_eq} = L_f \left[\dot{I}_{gq}^* + \frac{R_f}{L_f} \times I_{gq} + \omega_g \times I_{gd} + \frac{V_{gq}}{L_f} \right] \\ V_{fq_N} = K_{fq} \times \text{Smooth}(S(I_{rq})) \text{ with } K_{fq} > 0 \end{cases} \quad (46)$$

where I_{gq}^* is produced by the reactive power Q_{g-ref} that is fixed to zero to reach the unity power factor control, while I_{gd}^* is generated by the DC-link voltage regulator, as shown in Figure 5.

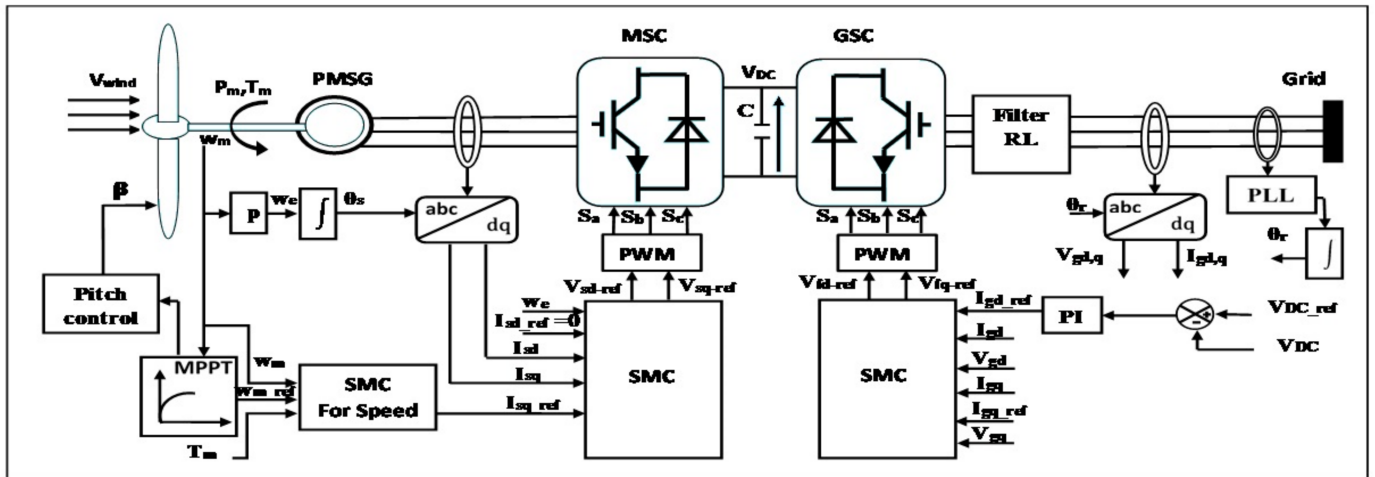


Figure 5. System control configuration.

3.3. Stability Analysis of the Proposed SMC

In this section, the global stability condition of the proposed SMC for the MSC and GSC, the Lyapunov stability function is introduced as follows [44–47]:

$$\begin{cases} V_{MSC} = \frac{1}{2} (S_{Isd}^2 + S_{Isq}^2 + S_{wmec}^2) \\ V_{GSC} = \frac{1}{2} (S_{Igd}^2 + S_{I_gq}^2) \end{cases} \quad (47)$$

where the Lyapunov stability function V_{MSC} is chosen for the MSC, while V_{GSC} is selected for the GSC.

The sliding mode stability is ensured if the Lyapunov function derivative is negative, as follows [45,47]:

$$\begin{cases} \dot{V}_{MSC} < 0 \\ \dot{V}_{GSC} < 0 \end{cases} \quad (48)$$

Hence, taking the time derivative of V_{MSC} and V_{GSC} , the obtained equations are as follows:

$$\begin{cases} \dot{V}_{MSC} = S_{Isd} \times \dot{S}_{Isd} + S_{Isq} \times \dot{S}_{Isq} + S_{wmec} \times \dot{S}_{wmec} \\ \dot{V}_{GSC} = S_{Igd} \times \dot{S}_{Igd} + S_{I_gq} \times \dot{S}_{I_gq} \end{cases} \quad (49)$$

When each derivative surface $\dot{S}(X)$ replacing with its expression, Equation (50) becomes:

$$\begin{cases} \dot{V}_{MSC} = S_{Isd} \times \left[\dot{I}_{sd}^* + \frac{R_s}{L_d} \times I_{sd} - \omega_e * \frac{L_q}{L_d} * I_{sq} - \frac{V_{sd}}{L_d} \right] + S_{Isq} \times \left[\dot{I}_{sq}^* + \frac{R_s}{L_q} \times I_{sq} + \omega_e \times \frac{L_d}{L_q} \times I_{sd} + \omega_e \times \frac{\partial f}{L_q} - \frac{V_{sq}}{L_q} \right] \\ \quad + S_{wmec} \times \left[\dot{\Omega}_{mec}^* + \frac{f}{J_{tot}} \times \Omega_{mec} + \frac{\mu}{J_{tot}} \times I_{sq} - \frac{T_{turb}}{J_{tot}} \right] \\ \dot{V}_{GSC} \\ = S_{Igd} \times \left[\dot{I}_{gd-ref} + \frac{R_f}{L_f} \times I_{gd} - \omega_g \times I_{gq} + \frac{V_{gd}}{L_f} - \frac{V_{fd}}{L_f} \right] + S_{I_gq} \times \left[\dot{I}_{gq-ref} + \frac{R_f}{L_f} \times I_{gq} + \omega_g \times I_{gd} + \frac{V_{gq}}{L_f} - \frac{V_{fq}}{L_f} \right] \end{cases} \quad (50)$$

Substituting Equations (38), (39), (41), (46), and (47) into Equation (51) gives the following:

$$\begin{cases} \dot{V}_{MSC} = -K_d \times S_{Isd} \times \text{Smooth}(S(I_{sd})) - K_q \times S_{Isq} \times \text{Smooth}(S(I_{sq})) - \\ \quad K_{\Omega_{mec}} \times S_{\omega_{mec}} \times \text{Smooth}(S(\Omega_{mec})) \\ \dot{V}_{GSC} = -K_{fd} \times S_{Igd} \times \text{Smooth}(S(I_{rd})) - K_{fq} \times S_{I_gq} \times \text{Smooth}(S(I_{rq})) \end{cases} \quad (51)$$

Finally, by replacing $\text{Smooth}(S(X))$ with its expression, Equation (52) becomes the following:

$$\begin{cases} \dot{V}_{MSC} = -K_{\Omega_{mec}} \times |S_{\omega_{mec}}| - K_d \times |S_{Isd}| - K_q \times |S_{Isq}| \\ \dot{V}_{GSC} = -K_{fd} \times |S_{Igd}| - K_{fq} \times |S_{I_gq}| \end{cases} \quad (52)$$

So, with $K_{\Omega_{mec}} > 0$, $K_d > 0$ and $K_q > 0$; $\dot{V}_{MSC} < 0$ and with $K_{fd} > 0$, $K_{fq} > 0$; $\dot{V}_{GSC} < 0$. Therefore, the Lyapunov condition is satisfied, and the main objectives of the proposed control are achieved.

The PSMC design is shown in Figure 5.

4. Simulation Results & Analysis

In this section, the proposed technique of the whole system has been simulated in the MATLAB/Simulink environment to evaluate its performance in a dynamic regime. The wind speed varies between 5 m/s and 9 m/s for 15 s, as shown in Figure 6. Furthermore, a comparison between the proposed PSMC and other controls has been performed to reveal the superiority of the proposed PSMC (Appendix A Tables A1 and A2) (Figure 6).

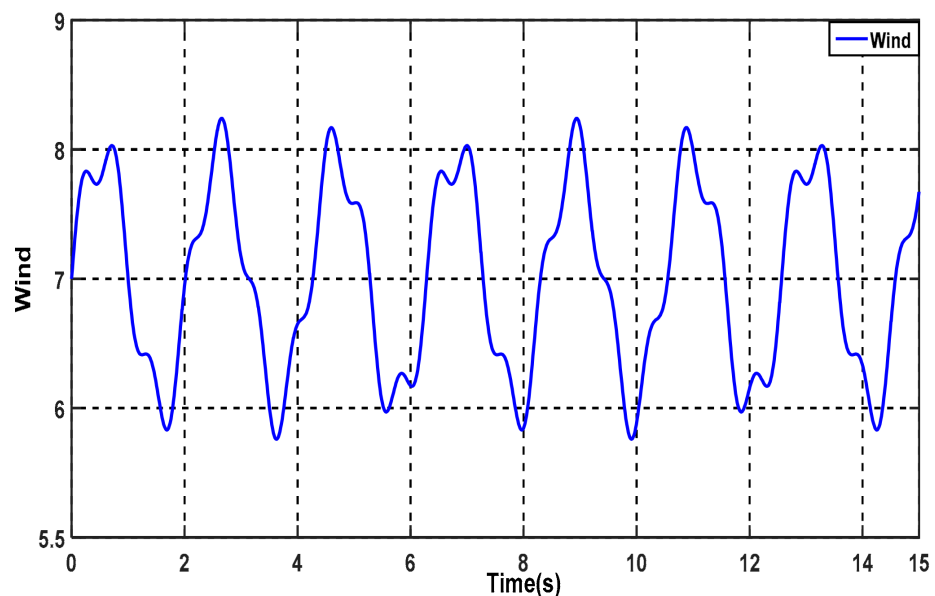


Figure 6. Wind speed profile.

From Figure 7a, we can observe that the power coefficient C_p and the specific speed λ are almost equal to their optimal reference values of 0.48 and 8, respectively, throughout the simulation period. Additionally, the mechanical speed (Figure 7b) of the PMSG ω_{mec} is the image of the wind profile, which follows its reference correctly. Figure 7c shows that the mechanical power P_{mec} has the same shape as the wind profile. Furthermore, Figure 7d shows that the electromagnetic torque T_{em} perfectly follows the optimum torque imposed by the maximum power point tracking algorithm. These results prove the performances of

the MPPT control, which allows us to exploit the maximum wind energy to produce the maximum of the electrical energy, as already mentioned in Section 2.

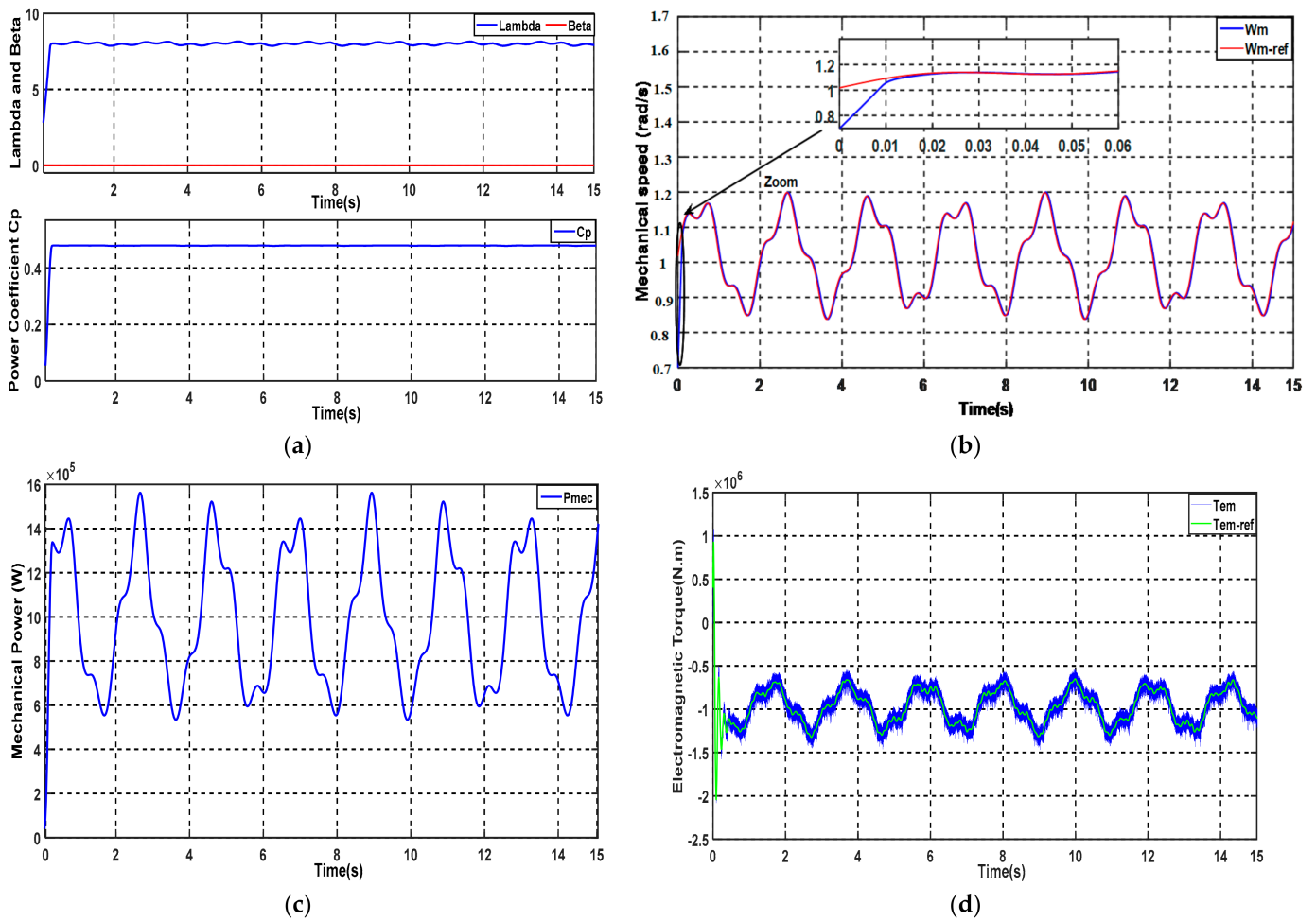


Figure 7. Performance of the system using the MPPT strategy: (a) tip speed ratio λ (lambda), Beta β and power coefficient (Cp), (b) mechanical speed (W_{mec}) of the PMSG, (c) mechanical power (P_{mec}), and (d) electromagnetic torque (T_{em}).

It can be seen from Figure 8a,b that the stator powers (P_s and Q_s) track their reference values with a high accuracy for both types of control. It can also be seen that the proposed control PSMC offers a better performance than that of the classical control CSMC in terms of oscillation, response time, and disturbance rates, while the reactive power Q_s (Figure 8b) of both controllers remains zero, indicating that the operation is with a unitary power factor, as shown in Figure 8b.

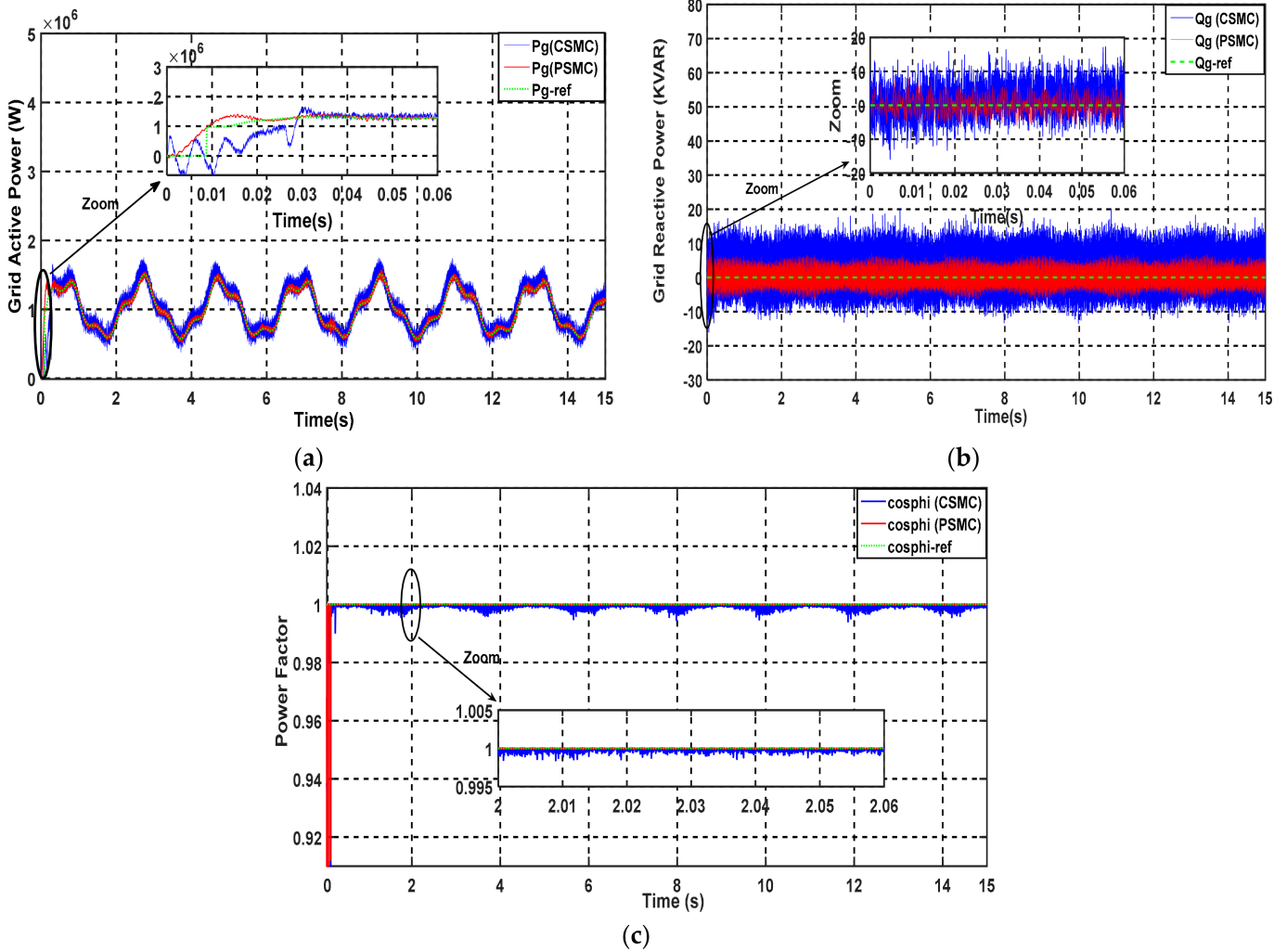


Figure 8. (a) Grid active power, (b) grid reactive power, and (c) power factor $\cos\phi$.

Compared to the classic technique, Figure 9 shows that the DC bus voltage remains stable given the variation in the wind.

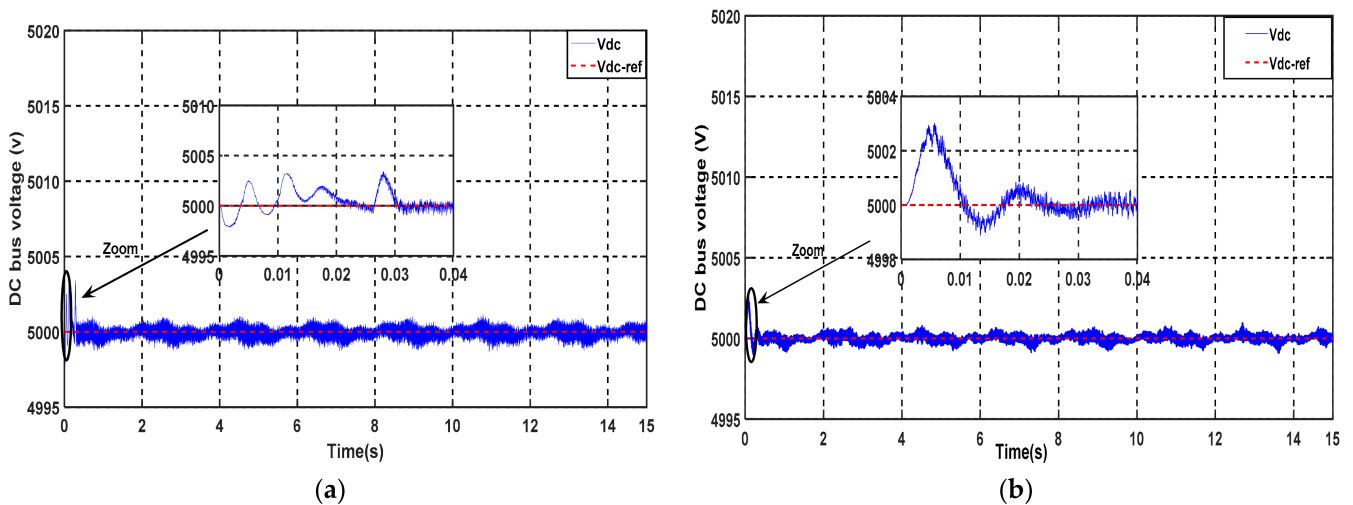


Figure 9. DC link voltage: (a) using CSMC and (b) using PSMC.

It can be seen from Figure 10 that the injected current amplitude varies with the wind speed variation, with a fixed frequency of 50 Hz, better sinusoidal waveform, and a lower ripple rate under PSMC control than that of the CSMC control. It can also be seen that the voltage and the injected currents are in phase, meaning that a power factor close to one is achieved.

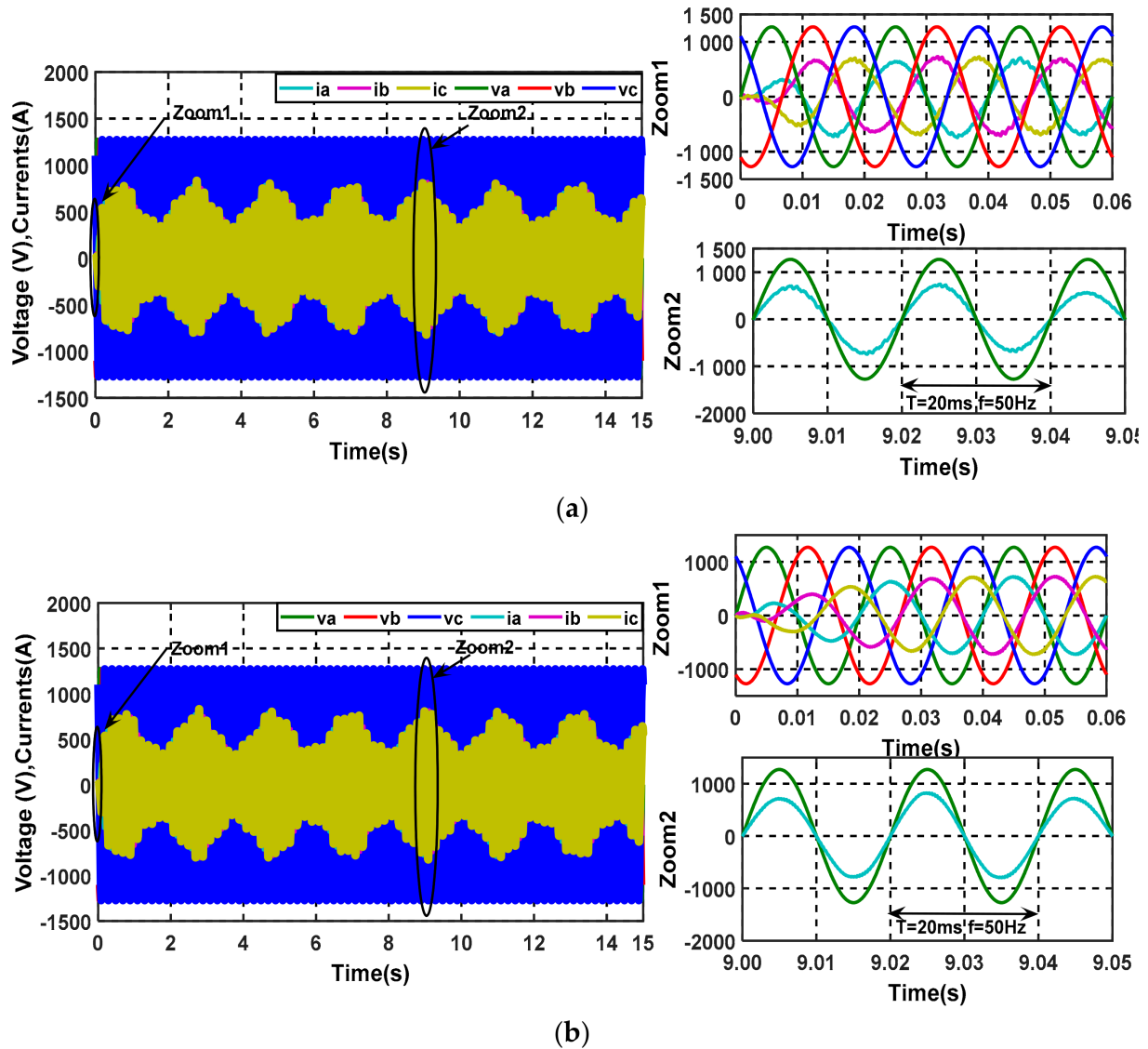


Figure 10. Grid voltage and injected current: (a) using the CSMC strategy and (b) using the PSMC strategy.

On the other hand, to study the effect of both controls on the quality of the signal supplied to the grid, a harmonic analysis of the grid current was carried out, as shown in Figure 11.

Figure 11 shows that the total harmonic distortion reached by the proposed PSMC control (Figure 11b) was considerably reduced (THD = 1.25%) compared to the result obtained by CSMC (THD = 3.06%; Figure 11a).

To get a clear view of the proposed control advantages, the previous comparison between the classical sliding mode and the proposed control is summarized in Table 1. It can be seen from this table that the proposed PSMC technique provides a great performance, which is especially included in the significant reduction in the chattering, good setpoint tracking, small response time, and high quality of the injected current.

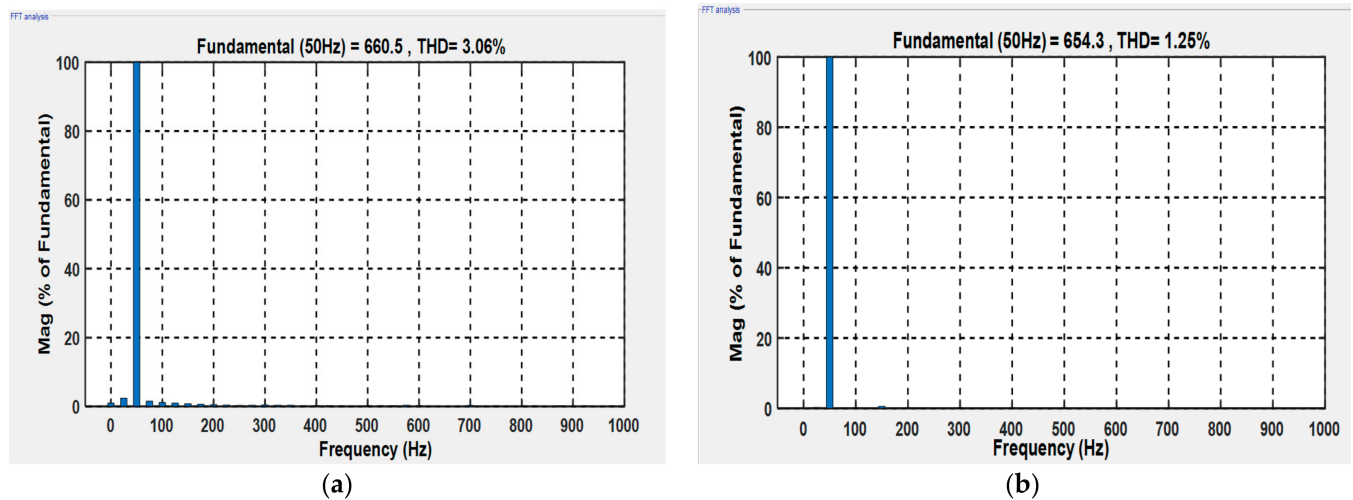


Figure 11. (a) THD using CSMC and (b) THD using PSMC.

Table 1. Performance Comparison Between the conventional SMC and the proposed approach for the WECS overtime period.

Performance	CSMC Technique	PSMC Technique
Set-point tracking %	80	99
Error %	0.31	0.15
Response time V_{dc} (ms)	32	22
Overshoot of V_{dc} %	0.096	0.05
Variation band of Q_r (KVAR)	25	15
Power efficiency (P_r/P_{mec}) %	99.60	99.75
Power Factor	1	1
THD of injected current (%)	3.06	1.25

A comparison of the results between the developed control and other recent studies is shown in Table 2. Although the error is minimized compared to [36,37], the biggest advantage of this control is the significant efficiency, and the overshoot was reduced compared to [28]. Comparing the $\cos\varphi$ of this study with [34,38], it is remarkable that the $\cos\varphi$ was increased in a very significant way for the controls proposed.

Table 2. Performance comparisons.

Publication	Technic methods	Efficiency	Error	Overshot	Cos φ	Robustness
[34]	PI neural controller	93.5	0.15%	0%	0.997	Moderate-high
	PI Fuzzy controller	93.99	0.14%	0%	0.974	Moderate-high
[28]	DTC-classical	92.13	0.32%	5%	0.983	Moderate-high
	DTC-GA-based PI	92.07	0.12%	1%	0.978	Moderate-high
[36]	SMC	91.14%	0.3%	-	-	Medium
[37]	Integral SMC	92.45%	0.2%	-	-	High
[38]	Fractionalorder SMC	98.6%	0.3%	-	-	High
Proposal technique	PSMC	98.99	0.12%	0%	0.995	High

5. Conclusions

This work provided a robust sliding mode control based on a unique smooth continuous function approach to cope with the chattering problem associated with the conventional sliding mode control (CSMC). The control approach is applied to a variable wind speed based on a permanent magnet synchronous generator. Moreover, the finest MPPT control approach combined with a pitch angle control was carried out to limit the power extraction above the rated wind speed and to insure wind turbine safety. The performance of the proposed PSMC was validated using a simulation test under varied wind speeds in the MATLAB/Simulink environment. The simulation data and the comparative analysis demonstrated that the recommended control is suitable for a wind power conversion system based on the PMSG variable speed.

Author Contributions: Conceptualization, B.M.; methodology, B.M.; software, B.M.; validation, B.M. and B.B.; formal analysis, B.M.; investigation, B.M.; resources, B.M. and M.M.; data curation, B.M. and M.E.M.; writing—original draft preparation, B.M.; writing—review and editing, J.F.A.-A., S.M. and M.B.; visualization, B.M. and M.K.; supervision, J.F.A.-A., M.T., S.M., B.B. and M.M.; project administration, B.B.; funding acquisition, J.F.A.-A. and S.M. All authors have read and agreed to the published version of the manuscript.

Funding: Taif University Researchers Supporting Project number (TURSP-2020/211), Taif University, Taif, Saudi Arabia.

Institutional Review Board Statement: Not applicable.

Informed Consent Statement: Not applicable.

Data Availability Statement: Not applicable.

Acknowledgments: The authors are grateful for the support of Taif University Researchers Supporting Project number (TURSP-2020/211), Taif University, Taif, Saudi Arabia.

Conflicts of Interest: The authors declare no conflict of interest.

Nomenclature

Ω_t	Turbine speed
β	Pitch angle
ρ	Air density
S	Surface
R_s	Resistances of the stator
L_d, L_q	d, q -axis Inductances
T_{em}, C_{em}	Electromagnetic torque
C_r	Load torque available at a motor shaft
$(v_{sd}, v_{sq}), (i_{sd}, i_{sq}), (\psi_{sd}, \psi_{sq})$	d/q stator voltages, currents, and fluxes
$(v_{gd}, v_{gq}), (i_{gd}, i_{gq})$	d/q grid voltages and currents
$(v_{fd}, v_{fq}), (i_{fd}, i_{fq})$	Voltages and currents at the RL filter
V_{dc}	DC link voltage
P_{gen}, P_g	Generator and grid Active power
Q_{gen}, Q_g	Generator and grid reactive power

Appendix A

Table A1. Wind turbine system parameters.

PMSG Parameters		Wind Turbine Parameters	
Power Generator P	P = 2 MW	Radius of the turbine blade	R = 55 m
Number of pole	p = 75	Turbine and generator inertia moment	J = 1000 N.m
Stator Resistance	$R_s = 0.00625 \Omega$	Density of air	$\rho = 1.22 \text{ Kg/m}^3$
d -axis inductance	$L_d = 0.004229 \text{ h}$	Tip speed Ratio	$\lambda = 8$
q -axis inductance	$L_q = 0.004229 \text{ h}$	Optimal Power Coefficient	$C_p = 0.5$
Generator flux	$\Phi_f = 11.1464 \text{ wb}$		

Table A2. Controller Parameters.

Controller Parameters	
K_d	10
K_q	30
K_{fd}	500
K_{fq}	100

References

- Bossoufi, B.; Karim, M.; Taoussi, M.; Aroussi, H.A.; Bouderbala, M.; Motahhir, S.; Camara, M.B. DSPACE-based implementation for observer backstepping power control of DFIG wind turbine. *IET Electr. Power Appl.* **2020**, *14*, 2395–2403. [\[CrossRef\]](#)
- Youness, E.M.; Aziz, D.; Abdelaziz, E.G.; Jamal, B.; Najib, E.O.; Othmane, Z.; Khalid, M.; Bossoufi, B. Implementation and validation of backstepping control for PMSG wind turbine using dSPACE controller board. *Energy Rep.* **2019**, *5*, 807–821. [\[CrossRef\]](#)
- Hong, C.M.; Chen, C.H.; Tu, C.S. Maximum power point tracking-based control algorithm for PMSG wind generation system without mechanical sensors. *Energy Convers. Manag.* **2013**, *69*, 58–67. [\[CrossRef\]](#)
- Benamor, A.; Benchouia, M.T.; Srairi, K.; Benbouzid, M.E.H. A novel rooted tree optimization apply in the high order sliding mode control using super-twisting algorithm based on DTC scheme for DFIG. *Int. J. Electr. Power Energy Syst.* **2019**, *108*, 293–302. [\[CrossRef\]](#)
- Pan, C.; Shao, L. Wind energy conversion systems analysis of PMSG on offshore wind turbine using improved SMC and Extended State Observer. *Renew. Energy* **2020**, *161*, 149–161. [\[CrossRef\]](#)
- Boumar, N.; Labdai, S.; Boukroune, A. PSO–GSA based fuzzy sliding mode controller for DFIG-based wind turbine. *ISA Trans.* **2019**, *85*, 177–188. [\[CrossRef\]](#) [\[PubMed\]](#)
- Liu, J.; Zhou, F.; Zhao, C.; Wang, Z.; Aguirre-Hernandez, B. A PI-type sliding mode controller design for PMSG-based wind turbine. *Complexity* **2019**, *2019*, 2538206. [\[CrossRef\]](#)
- Soliman, M.A.; Hasanien, H.M.; Azazi, H.Z.; El-Kholy, E.E.; Mahmoud, S.A. An adaptive fuzzy logic control strategy for performance enhancement of a grid-connected PMSG-Based wind turbine. *IEEE Trans. Ind. Inform.* **2019**, *15*, 3163–3173. [\[CrossRef\]](#)
- Beddar, A.; Bouzekri, H.; Babes, B.; Afghoul, H. Experimental enhancement of fuzzy fractional order PI+I controller of grid connected variable speed wind energy conversion system. *Energy Convers. Manag.* **2016**, *123*, 569–580. [\[CrossRef\]](#)
- Aounallah, T.; Essounbouli, N.; Hamzaoui, A.; Bouchafaa, F. Algorithm on fuzzy adaptive backstepping control of fractional order for doubly-fed induction generators. *IET Renew. Power Gener.* **2018**, *12*, 962–967. [\[CrossRef\]](#)
- Yin, W.; Wu, X.; Rui, X. Adaptive robust backstepping control of the speed regulating differential mechanism for wind turbines. *IEEE Trans. Sustain. Energy* **2019**, *10*, 1311–1318. [\[CrossRef\]](#)
- Beniysa, M.; Idrissi, A.E.J.E.; Bouajaj, A.; Britel, M.R.; Ariwa, E. Neural network adaptive backstepping control via uncertainty compensation for PMSG-based variable-speed wind turbine: Controller design and stability analysis. *Wind Eng.* **2021**. [\[CrossRef\]](#)
- Matraji, I.; Al-Durra, A.; Errouissi, R. Design and experimental validation of enhanced adaptive second-order SMC for PMSG-based wind energy conversion system. *Int. J. Electr. Power Energy Syst.* **2018**, *103*, 21–30. [\[CrossRef\]](#)
- Xiong, L.; Li, P.; Ma, M.; Wang, Z.; Wang, J. Output power quality enhancement of PMSG with fractional order sliding mode control. *Int. J. Electr. Power Energy Syst.* **2020**, *115*, 105402. [\[CrossRef\]](#)
- Hostettler, J.; Wang, X. Sliding mode control of a permanent magnet synchronous generator for variable speed wind energy conversion systems. *Syst. Sci. Control Eng.* **2015**, *3*, 453–459. [\[CrossRef\]](#)
- Gautam, K.K.; Sankaranarayanan, V. Sliding mode control of surface mounted permanent magnet synchronous generator. *IFAC Proc. Vol.* **2014**, *47*, 1034–1038. [\[CrossRef\]](#)
- Ayadi, M.; Ben Salem, F.; Derbel, N. Sliding mode approach for blade pitch angle control wind turbine using PMSG under DTC. In Proceedings of the 2015 16th International Conference on Sciences and Techniques of Automatic Control and Computer Engineering (STA), Monastir, Tunisia, 21–23 December 2015; pp. 758–762. [\[CrossRef\]](#)
- Haq, I.U.; Khan, M.I.; Zeb, K. Siding Mode Control for PMSG based Wind Energy Conversion System connected to the grid. In Proceedings of the 2016 International Conference on Computing, Electronic and Electrical Engineering (ICE Cube), Quetta, Pakistan, 11–12 April 2016; pp. 277–282. [\[CrossRef\]](#)
- Benelghali, S.; Benbouzid, M.E.H.; Charpentier, J.F.; Ahmed-Ali, T.; Munteanu, I. Experimental validation of a marine current turbine simulator: Application sliding mode control. *IEEE Trans. Ind. Electron.* **2011**, *58*, 118–126. [\[CrossRef\]](#)
- Errouissi, R.; Al-Durra, A. A Novel PI-Type Sliding Surface for PMSG-Based Wind Turbine with Improved Transient Performance. *IEEE Trans. Energy Convers.* **2018**, *33*, 834–844. [\[CrossRef\]](#)
- Phan, D.H.; Huang, S.D. Super-twisting sliding mode control design for cascaded control system of pmsg wind turbine. *J. Power Electron.* **2015**, *15*, 1358–1366. [\[CrossRef\]](#)

22. Jaramillo-Lopez, F.; Kenne, G.; Lamnabhi-Lagarrigue, F. A novel online training neural network-based algorithm for wind speed estimation and adaptive control of PMSG wind turbine system for maximum power extraction. *Renew. Energy* **2016**, *86*, 38–48. [[CrossRef](#)]
23. El Mourabit, Y.; Derouich, A.; Allouhi, A.; El Ghzizal, A.; El Ouanjli, N.; Zamzoumyes, O. Sustainable production of wind energy in the main Morocco's sites using permanent magnet synchronous generators. *Int. Trans. Electr. Energ. Syst.* **2020**, *30*, e12390. [[CrossRef](#)]
24. Yin, X.-X.; Lin, Y.-G.; Li, W.; Gu, Y.-J.; Liu, H.-W.; Lei, P.-F. A novel fuzzy integral sliding mode current control strategy for maximizing wind power extraction and eliminating voltage harmonics. *Energy Elsevier* **2015**, *85*, 677–686. [[CrossRef](#)]
25. Meghni, B.; Dib, D.; Azar, A.T. A second-order sliding mode and fuzzy logic control to optimal energy management in wind turbine with battery storage. *Neural Comput. Appl.* **2017**, *28*, 1417–1434. [[CrossRef](#)]
26. Beltran, B.; Benbouzid, M.E.H.; Ahmed-Ali, T. Second-Order Sliding Mode Control of a Doubly Fed Induction Generator Driven Wind Turbine. *IEEE Trans. Energy Convers.* **2012**, *27*, 261–269. [[CrossRef](#)]
27. Yang, B.; Yu, T.; Shu, H.; Dong, J.; Jiang, L. Robust Sliding-mode Control of Wind Energy Conversion Systems for Optimal Power Extraction via Nonlinear Perturbation Observers. *Appl. Energy* **2018**, *210*, 711–723. [[CrossRef](#)]
28. Benamor, A.; Benchouia, M.T.; Srairi, K.; Benbouzid, M.E.H. A new rooted tree optimization algorithm for indirect power control a wind turbine based on a powered double induction generator. *ISA Trans.* **2019**, *88*, 296–306. [[CrossRef](#)]
29. Freire, N.; Estima, J.; Cardoso, A. A Comparative Analysis of PMSG Drives Based on Vector Control and Direct Control Techniques for Wind Turbine Applications. *Electr. Rev.* **2012**, *88*, 184–187.
30. Zribi, M.; Alrifai, M.; Rayan, M. Sliding Mode Control of a Variable—Speed Wind Energy Conversion System Using a Squirrel Cage Induction Generator. *Energies* **2017**, *10*, 604. [[CrossRef](#)]
31. Gonzalez, L.; Figueres, E.; Garcera, G.; Carranza, O. Maximum-power-point tracking with reduced mechanical stress applied to wind energy conversion systems. *Appl. Energy* **2010**, *87*, 2304–2312. [[CrossRef](#)]
32. Mousa, H.H.; Youssef, A.R.; Mohamed, E.E. Model predictive speed control of five-phase permanent magnet synchronous generator-based wind generation system via wind-speed estimation. *Int. Trans. Electr. Energy Syst.* **2019**, *29*, e2826. [[CrossRef](#)]
33. Jena, N.K.; Mohanty, K.B.; Pradhan, H.; Sanyal, S. A comparison between PI SMC used for decoupled control of PMSG in a variable speed wind energy system. In Proceedings of the 2015 International Conference on Energy, Power and Environment: Towards Sustainable Growth (ICEPE), Shillong, India, 12–13 June 2015; pp. 1–6.
34. Jin, N.; Wang, X.; Wu, X. Current Sliding Mode Control with a Load Sliding Mode Observer for Permanent Magnet Synchronous Machines. *J. Power Electron.* **2014**, *14*, 105–114. [[CrossRef](#)]
35. Bossoufi, B.; Karim, M.; Lagrioui, A.; Taoussi, M.; Derouich, A. Observer Backstepping control of DFIG-Generators for Wind Turbines Variable-Speed: FPGA-Based Implementation. *Renew. Energy J.* **2015**, *81*, 903–917. [[CrossRef](#)]
36. Rhaili, S.E.; Abbou, A.; Marhraoui, S.; Moutchou, R.; El Hichami, N. Robust Sliding Mode Control with Five Sliding Surfaces of Five-Phase PMSG Based Variable Speed Wind Energy Conversion System. *Int. J. Intell. Eng. Syst.* **2020**, *13*, 346–357. [[CrossRef](#)]
37. Mousa, H.H.H.; Youssef, A.R.; Mohamed, E.E.M. Optimal Power Extraction Control Schemes for Five-Phase PMSG Based Wind Generation Systems. *Eng. Sci. Technol. Int. J.* **2020**, *23*, 144–155. [[CrossRef](#)]
38. Rhaili, S.E.; Abbou, A.; Hichami, N.E.; Marhraoui, S.; Choja, H. Mawimum power extraction of five-phase PMSG WECS by adopting and improved fractional order sliding mode strategy. *Jilin DaxueXuebao* **2021**, 55–74. [[CrossRef](#)]
39. Bouderbala, M.; Bossoufi, B.; Deblecker, O.; AlamiAroussi, H.; Taoussi, M.; Lagrioui, A.; Motahhir, S.; Masud, M.; Alraddady, F.A. Experimental Validation of Predictive Current Control for DFIG: FPGA Implementation. *Electronics* **2021**, *10*, 2670. [[CrossRef](#)]
40. Bossoufi, B.; Karim, M.; Taoussi, M.; AlamiAroussi, H.; Bouderbala, M.; Deblecker, O.; Motahhir, S.; Nayyar, A.; Massud, M. Rooted Tree Optimization for Backstepping Power Control of DFIG Wind Turbine: dSPACE Implementation. *IEEE Access* **2021**, *9*, 26512–26522. [[CrossRef](#)]
41. AlamiAroussi, H.; El Ziani, M.; Bouderbala, M.; Bossoufi, B. Enhancement of the direct power control applied to DFIG-WECS. *Int. J. Electr. Comput. Eng.* **2020**, *10*, 1511–1520.
42. Hammoumi, D.; Bakkali, C.E.L.; Karim, M.; Taoussi, M.; Ouanjli, N.E.L.; Bossoufi, B. Direct controls for wind turbine with PMSG used on the real wind profile of Essaouira-Morocco city. *Indones. J. Electr. Eng. Comput. Sci.* **2019**, *16*, 1229–1239. [[CrossRef](#)]
43. Aroussi, H.A.; El Ziani, M.; Bouderbala, M.; Bossoufi, B. Improvement of Direct Torque Control Applied To Doubly Fed Induction Motor under Variable Speed. *IJPEDS Int. J. Power Electron. Drive Syst.* **2020**, *11*, 1511–1520. [[CrossRef](#)]
44. El Mahfoud, M.; Bossoufi, B.; ElOunjli, N.; Mahfoud, S.; Taoussi, M. Improved Direct Torque Control of Doubly Fed Induction Motor Using Space Vector Modulation. *Int. J. Intell. Eng. Syst.* **2021**, *14*, 177–188. [[CrossRef](#)]
45. El Karaoui, I.; Maaroufu, M.; Bossoufi, B. Fuzzy Sliding Mode Power Control for Wind Power Generation System Connected to the Grid. *IJPEDS Int. J. Power Electron. Drive Syst.* **2021**, *11*, 11–25.
46. Majout, B.; Abrahami, D.; Ihedrane, Y.; El Bakkali, C.; Karim, M.; Bossoufi, B. Improvement of Sliding Mode Power Control Applied to Wind Power Generation system based on DFIG. *IJPEDS Int. J. Power Electron. Drive Syst.* **2021**, *12*, 441–452.
47. Zine Laabidine, N.; Errahout, A.; Bakkali, C.E.L.; Karim, M.; Bossoufi, B. Sliding Mode Control Design of Wind Power Generation system based on PMSG. *IJPEDS Int. J. Power Electron. Drive Syst.* **2021**, *12*, 393–403.